NASA TECHNICAL NOTE

NASA TN D-3136

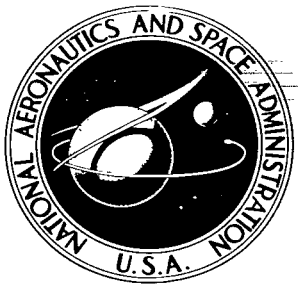

NASA TN D-3136

INVESTIGATION OF THE STARTING CHARACTERISTICS OF THE M-1 ROCKET ENGINE USING THE ANALOG COMPUTER

by John R. Szuch, Leon M. Wenzel, and Robert J. Baumbick

Lewis Research Center
Cleveland, Ohio

NATIONAL AERONAUTICS AND SPACE ADMINISTRATION - WASHINGTON, D. C. - DECEMBER 1965

INVESTIGATION OF THE STARTING CHARACTERISTICS OF THE M-1 ROCKET ENGINE USING THE ANALOG COMPUTER

By John R. Szuch, Leon M. Wenzel, and Robert J. Baumbick

Lewis Research Center
Cleveland, Ohio

NATIONAL AERONAUTICS AND SPACE ADMINISTRATION

For sale by the Clearinghouse for Federal Scientific and Technical Information
Springfield, Virginia 22151 – Price $2.00

INVESTIGATION OF THE STARTING CHARACTERISTICS OF THE M-1 ROCKET ENGINE USING THE ANALOG COMPUTER

by John R. Szuch, Leon M. Wenzel, and Robert J. Baumbick

Lewis Research Center

SUMMARY

The purpose of this investigation was to study the starting characteristics of the M-1 engine system by using an analog computer simulation. It is further intended that this report serve as a guide to others undertaking liquid rocket propulsion system studies on the analog computer. The formulation of the M-1 system equations is discussed in detail, and a summary of the resultant equations is included in an appendix. To evaluate the starting characteristics of the engine, the times required to reach 90 percent of the rated thrust chamber pressure and fuel pump stall margin were selected as figures of merit. The following information was obtained from the analog simulation:

(1) The effect of ambient pressure on the engine start transient was negligible with pressures ranging from zero to atmospheric.

(2) Stall margin could, in general, be increased by increasing the recirculation valve area at the cost of increased acceleration time. Stall margin was found to be a slight inverse function of recirculation line diameter. A decrease in acceleration time, together with an increase in stall margin, was obtained by using a 4-inch line with a recirculation valve area and spring rate greater than nominal.

(3) Failure of the recirculation valve to close during the start transient resulted in a steady-state thrust chamber mixture ratio near stoichiometric.

(4) For any given inlet line configuration, thrust chamber to propellant tank pressure ratios can be obtained from engine impedance characteristics measured on the analog. Over the expected range of possible POGO-stick-type oscillations (0 to 20 cps), the engine impedances were approximately constant with the dominant dynamics expected from the inlet lines.

INTRODUCTION

The purpose of this investigation was to study and predict the dynamic characteris-

tics of the M-1 engine system by using an analog computer simulation. It is further intended that this report serve as a guide to others undertaking studies of liquid rocket propulsion systems on analog computers.

A computer simulation, when properly used, can be a powerful tool in guiding an engine development program. It provides an easy and economical means for evaluating various design approaches and forewarns the designer of possible problem areas before costly hardware is developed and subsequently scrapped. Once a qualitative design is established, the system may be "tuned" for optimum performance by varying the system parameters about their design values.

Although the digital computer provides the design engineer with higher numerical accuracy, the analog computer offers the following advantages over the digital as a design tool: (1) the system equations are solved continuously rather than at discrete intervals of time; (2) the engineer is able to observe the effects of changes in the system as they occur rather than in numerical form at some later date; and (3) visual displays of system behavior, such as engine start transients, etc., give the engineer an added "feel" for his problem.

Since a major portion of the M-1 engine hardware was still in the design stage, design information, rather than experimental data, was used to simulate the system components. Wherever possible, information from other engines was used to aid in the simulation. For example, the simulation of the RL-10 engine, for which there was excellent agreement with test data (ref. 1), provided invaluable simulation experience and information. Several of the approximations and assumptions, described in the analysis, were based on experience gained through the RL-10 engine simulation. Acknowledgement is made to Aerojet General Corporation for their cooperation in providing the necessary design information in addition to results from their digital computer simulation of the M-1 system.

Under limitations of using design data rather than test data, the work reported herein pertains to engine simulation in general and the development of the M-1 simulation in particular. To aid in the design of facilities for engine testing, the effect of ambient pressure on the start transient was determined for pressures ranging from zero to atmospheric. To optimize the design of the fuel pump recirculation system, parametric studies on line diameter, valve diameter, and valve spring rate were conducted. In addition, a failure analysis was performed on the recirculation valve to determine the criticality of such a failure. Engine transfer functions were determined that will be useful in vehicle design studies once tank and inlet line data become available.

EQUIPMENT AND PROCEDURE

A schematic of the M-1 system is shown in figure 1. The engine is powered by liquid

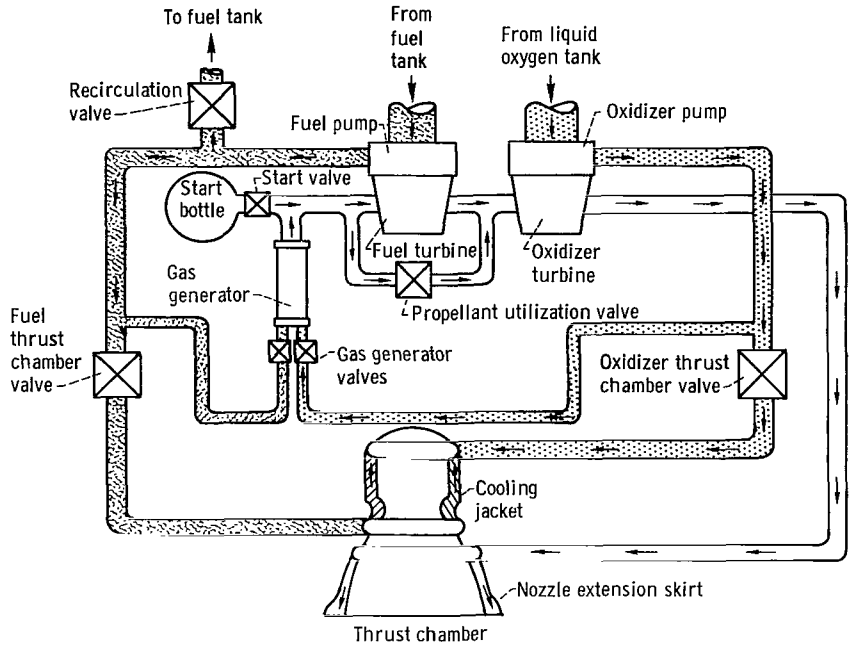

Figure 1. - Schematic of M-1 rocket engine system.

hydrogen and liquid oxygen supplied by the two pumps and is regeneratively cooled by the liquid hydrogen that passes through the cooling jacket before entering the thrust chamber. Initial pump spinup is accomplished by supplying high pressure helium gas from the start bottle to the turbines. After the gas generator ignites, the helium flow rate gradually decreases as the gas generator burnt products supply the energy for acceleration and steady-state operation of the turbines. Turbine discharge gases are expelled through the nozzle extension skirt to provide skirt cooling. Rising fuel pump discharge pressure closes the fuel pump recirculation valve, which is initially held open by spring forces. This valve provides both prestart pump cooling and a low flow impedance downstream of the fuel pump during the initial phase of the start transient.

The M-1 analog simulation utilized the analog computer facility at the Lewis Research Center. Three computer consoles were used with all mode controls slaved to one console. Approximately 250 amplifiers, 50 multipliers, 20 variable diode-function generators, and 5 fixed diode-function generators were used in the M-1 simulation. Start transients were recorded on three 8-channel strip-chart recorders. Transient traces were plotted on both oxidizer and fuel pump maps when needed by using X-Y plotters. Program expansion and refinement, whenever necessary, was accomplished by using an additional console.

Since the computers used are 100-volt devices, all system variables were scaled so as not to exceed that value. Included in appendix B is a summary of the voltage scaling used in this simulation. To facilitate the programing and recording of the start transient,

the system was slowed down (time scaled) by a factor of 100. The sequencing of system valves was accomplished by using pump discharge pressure to drive comparator-driven relays, while the start valve opening and closing was accomplished by manually throwing a switch on the computer control panel.

Because of operational problems, the start transient could not be initiated on the computer from an absolute zero condition. For example, an attempt to compute initial pressure ratios would result in fallacious results since the electronic dividers are inaccurate for very small input voltages, small errors being greatly magnified. To avoid this situation, the problem was started with a small helium flow (0.5 percent of maximum) through the hot gas ducts with appropriate initial conditions on the problem variables.

The engine transfer functions were obtained experimentally by using the computer model, minus the inlet lines, and a sinusoidal transfer function analyzer. The latter device generates its own test signal (input) and receives whatever output signal is of interest (e.g., thrust chamber pressure). The analyzer then computes the magnitudes and phases of the Fourier transforms of both input and output signals at test frequencies selected by the operator. Since the problem was time scaled by a factor of 100, and since the frequency range of interest was 1 to 100 cps, the analyzer was operated from 0.01 to 1.0 cps.

ANALYSIS

The first step in developing any analog program is the formulation of an analytical model. This formulation will, in general, result in a set of simultaneous equations. Since the analog computer can handle only ordinary differential equations, certain approximations and manipulations are necessary when preparing a problem for the analog computer. For example, one-dimensional heat flow problems result in partial differential equations, which can be handled by means of finite-difference techniques (ref. 2). In a complex system simulation, such as the M-1, approximations must also be made to conserve computing equipment. Engineering judgment is required to economize on equipment where the result will not invalidate or seriously compromise the overall problem accuracy.

A block diagram of the M-1 system is shown in figure 2. To facilitate the program development, the M-1 engine system was considered as being a composite of three sections. These sections were the helium and hot gas driving system, the main propellant feed system, and the cooling jacket and main engine assembly. After deriving the necessary equations, each section was built up on the computer independently. The simulation was then completed by closing the various interconnecting loops. In the following paragraphs, these sections will be discussed in detail in the order just mentioned.

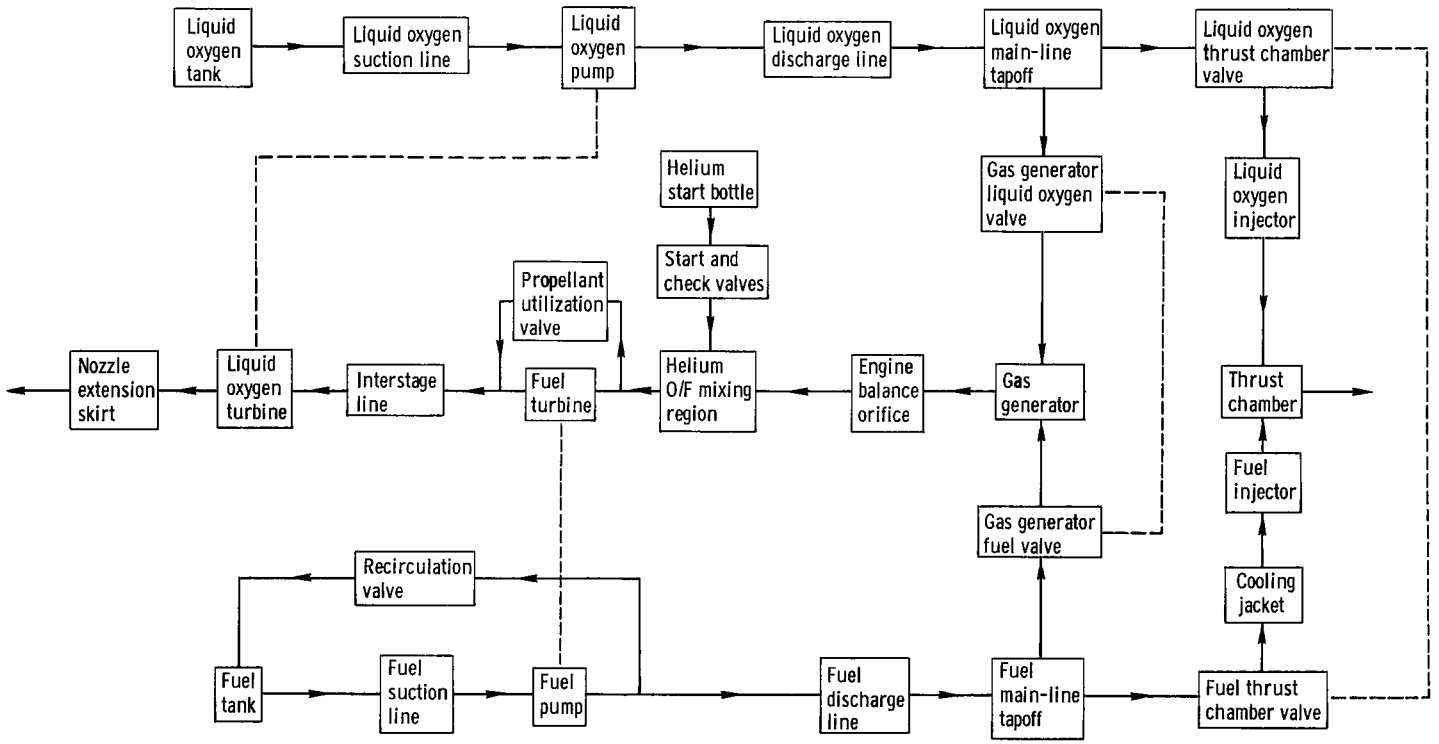

Figure 2. - Block diagram of M-1 engine system.

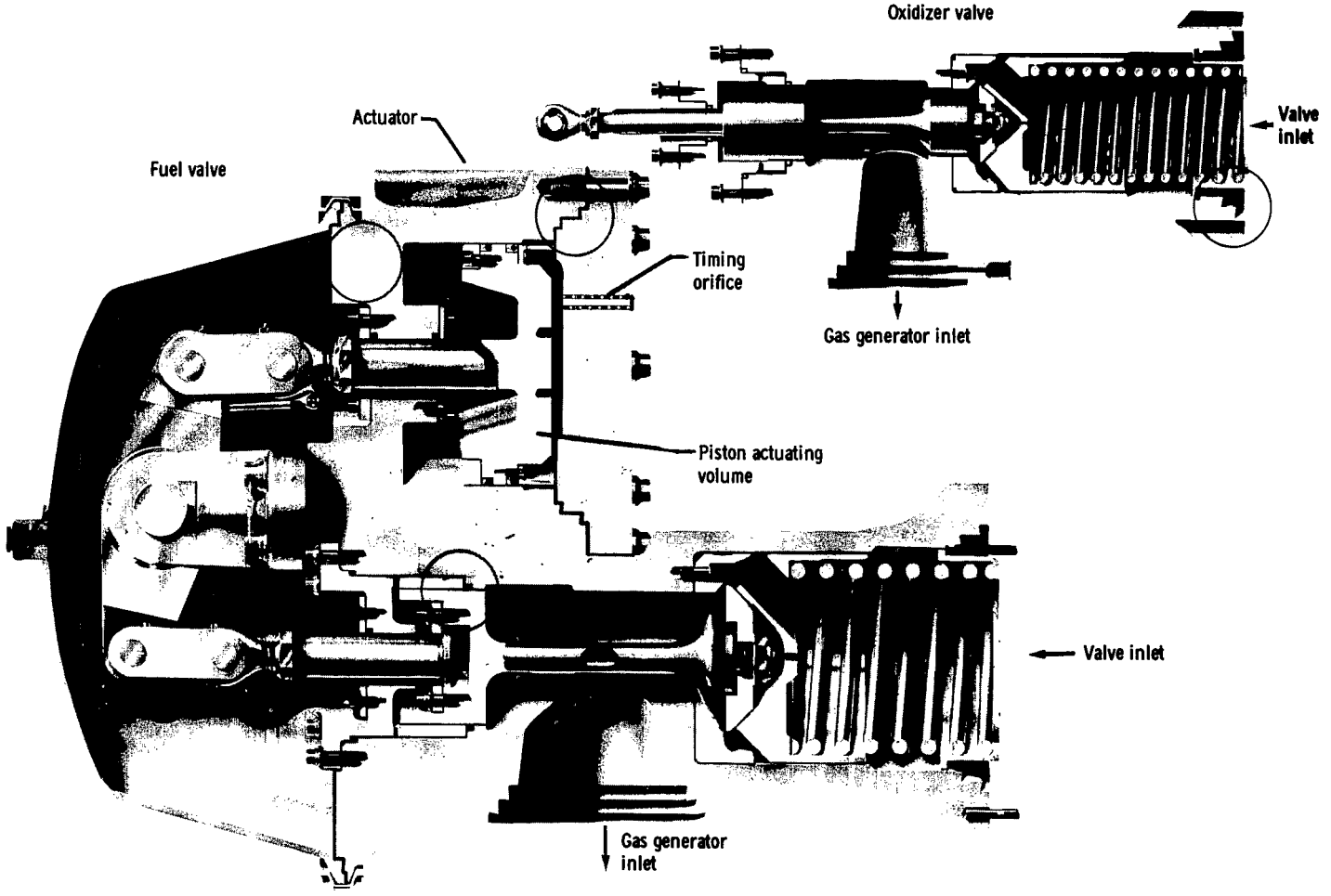

Figure 3. - M-1 Gas generator valve configuration.

Helium and Hot Gas Drive Section

On startup, the M-1 turbines derive their power successively from the flow of helium from the start bottle, a mixture of helium and gas generator burnt products, and finally, all burnt products. The burnt products are supplied by the gas generator, which is fed by liquid hydrogen and oxygen tapped from the main propellant feed lines. All losses between the main-line tapoff and the gas generator chamber were lumped together because of equipment limitations. These losses (lines, valving, manifolds) were assumed to be proportional to the square of flow rate (ref. 3).

The gas generator valve configuration is shown in figure 3. Both the fuel and oxidant valves are driven by the same actuating piston and are opened by the rising fuel pump discharge pressure. An economical simulation of the valve dynamics was made by neglecting valve forces, assuming that the timing orifice is always choked, and neglecting the change in the piston actuating volume V_{PA} due to the piston travel. These assumptions, together with the prescribed relation between valve contours and valve stroke, led to the following equations, which are easily implemented on the computer:

Valve stroke:

$$y_{GGV} = K_1 \int_0^t P_{dFP}\, dt - K_2 \tag{1}$$

Gas generator oxidant flow rate:

$$\dot{W}_{GGO} = \left(C_d A\right)_O \left[2g\rho_O \left(\Delta P_{GGV}\right)_O\right]^{1/2} \tag{2}$$

Gas generator fuel flow rate:

$$\dot{W}_{GGF} = \left(C_d A\right)_F \left[2g\rho_F \left(\Delta P_{GGV}\right)_F\right]^{1/2} \tag{3}$$

All symbols are defined in appendix A.

The continuity equation (ref. 3) was used to compute the gas generator chamber pressure from the net instantaneous weight flow into the chamber, assuming a perfect gas after ignition and no combustion dead time. The gas properties in the gas generator chamber (i. e., C^*, R, and γ) were computed from the percent fuel entering the gas generator by using curve fitting techniques. Gas generator ignition was delayed until the liquid oxygen manifold was filled. The filling time was determined by integrating the gas generator oxidant flow rate until the weight stored in the manifold volume was equal to the capacity of that volume ($\rho_O V_{man}$).

An engine balance orifice (fig. 2) is located between the gas generator and the fuel

turbine manifold. The sizing of this orifice affects the distribution of pressures across the fuel and oxidant turbines, which allows the thrust level to be adjusted by means of the pump driving powers. The orifice was assumed never to choke, and the flow rate through the orifice was computed by using equation (4). To account for the backflow of helium through the orifice during the first portion of the start transient, the fluid density at the orifice was computed from the average of the upstream and downstream pressures and the temperature downstream of the orifice (i.e., at the helium - O/F mixing region):

$$\dot{W}_{ORF} = \left(C_D A\right)_{ORF}\left(2g\rho_{ORF}\,\Delta P_{ORF}\right)^{1/2} \tag{4}$$

For the computation of both turbine flow rates, equation (4) proved to be inadequate due to the higher flow velocities. In the case of a high Mach number ($M > 0.3$) restriction (ref. 4, pp. 83 to 89), the flow must be treated as compressible, which requires a knowledge of static downstream pressures. For both turbines, it was necessary to relate static pressure to total pressure at the turbine exit. It was assumed that the static to total pressure ratios at the turbine exits were constant:

$$\frac{p_d}{P_d} = \left.\frac{p_d}{P_d}\right|_r = \text{constant} = K_r \tag{5}$$

over the range of Mach numbers encountered during the start transient ($M < 1.0$). This assumption allowed the computation of the turbine pressure ratios as follows:

$$\frac{p_d}{P_u} = K_r \frac{P_d}{P_u} \tag{6}$$

The use of the energy equation led to the following expression for the flow rate through the turbines in terms of the pressure ratios (ref. 4) at the nominal mixture ratio in the gas generator:

$$\left.\dot{W}_{TUR}\right|_r = \frac{P_u A_{TUR}}{\left(R_M T_u\right)^{1/2}}\left(K_r \frac{P_d}{P_u}\right)^{1/\gamma_r}\left\{\frac{2g\gamma_r}{\gamma_r - 1}\left[1 - \left(K_r \frac{P_d}{P_u}\right)^{(\gamma_r - 1)/\gamma_r}\right]\right\}^{1/2} \tag{7}$$

Equation (7) implies a pure impulse machine with no static pressure loss across the rotating elements. Although equipment limitations prevented any modification of the turbine flow rates due to variations from this condition, the resulting turbine torques were

continuously adjusted through turbine efficiencies, which were computed from equations supplied by the contractor.

To account for variations in the turbine flow rates due to changes in fluid properties, a curve fitting technique was used to obtain a first-order correction factor:

$$F(\gamma_M) = K_3 \frac{\gamma_M - 1}{\gamma_M} + K_4 \tag{8}$$

Combining equations (7) and (8) resulted in the following expression for the flow rate through the turbine (either fuel or oxidizer turbine):

$$\dot{W}_{TUR} = F(\gamma_M)\dot{W}_{TUR}\Big|_r \tag{9}$$

The flow rate through the propellant utilization valve (see fig. 2, p. 5) was computed in a similar fashion. This valve controls the mixture ratio in the thrust chamber by controlling the flow rate through the fuel turbine. The temperature drop across the propellant utilization valve was considered negligible.

In order to compute the main line flows, pump speeds, etc., it was necessary to compute the turbine torques. The following equations, derived from energy considerations and curve fitting techniques, summarize the methods used in computing the turbine torques and downstream temperatures (ref. 4):

$$\Delta h_{ID} = c_{pM} T_u \left[1 - \left(K_r \frac{P_d}{P_u} \right)^{(\gamma_M - 1)/\gamma_M} \right] \tag{10}$$

$$\Delta h_{ACT} = \eta_{TUR} \Delta h_{ID} \tag{11}$$

$$\eta_{TUR} = K_5 \left(\frac{u}{c} \right) + K_6 \left(\frac{u}{c} \right)^2 \tag{12}$$

$$u = \frac{\pi}{30} r_{TUR} N \tag{13}$$

$$c = (2gJ \Delta h_{ACT})^{1/2} \tag{14}$$

$$L_{TUR} = \frac{J}{2\pi} \dot{W}_{TUR} \frac{\Delta h_{ACT}}{N} \tag{15}$$

$$c_{pM}T_d = c_{pM}T_u - \Delta h_{ACT} \tag{16}$$

Fuel turbine:

$$c_{pM}T_u = c_{pM}T_M \tag{17a}$$

Oxidizer turbine:

$$c_{pM}T_u = c_{pM}T_M - \left(\frac{\dot{W}_{TUR}\,\Delta h_{ACT}}{\dot{W}_{TUR} + \dot{W}_{PUV}}\right)_F \tag{17b}$$

$$N = \frac{30}{\pi I}\int_0^t (L_{TUR} - L_P)dt \tag{18}$$

The determination of turbine torques, therefore, required continuous knowledge of the helium - O/F mixtures' temperature and gas constants. These were computed by averaging (by weight) the contributions of the helium and burnt products. The following equations summarize this averaging technique which is developed in detail in appendix C.

$$\beta = \frac{\dot{W}_{GGO} + \dot{W}_{GGF}}{\dot{W}_{GGO} + \dot{W}_{GGF} + \dot{W}_{HE}} \tag{19}$$

$$c_{pM} = \beta c_{pBP} + (1 - \beta)c_{pHE} \tag{20}$$

$$h_M = \beta h_{BP} + (1 - \beta)h_{HE} \tag{21}$$

$$R_M = \beta R_{BP} + (1 - \beta)R_{HE} \tag{22}$$

The nozzle extension skirt was considered to be a choked orifice with the flow rate through the skirt computed from the following equation:

$$\dot{W}_{SK} = \frac{A_{SK}P_{dOT}}{(R_M T_{dOT})^{1/2}}\left(\frac{2}{\gamma_M + 1}\right)^{1/(\gamma_M - 1)}\left(\frac{2g\gamma_M}{\gamma_M + 1}\right)^{1/2} \tag{23}$$

The helium gas is supplied by a start bottle (see fig. 2) initially at pressure P_i and temperature T_i. Upon opening of the start valve, the helium gas was assumed to expand isentropically. The pressure and temperature were then related (ref. 5) through the following equation:

$$T_{HE}P_{HE}^{(1-\gamma_{HE})/\gamma_{HE}} = T_iP_i^{(1-\gamma_{HE})/\gamma_{HE}} \tag{24}$$

The start valve was considered to be variable area restriction with the flow rate computed from equation (7). The static downstream pressure was assumed to be equal to the total pressure downstream of the valve ($M << 1.0$). The dynamics of the line between the check valve and the fuel turbine manifold were neglected. All losses associated with the start valve and check valve were lumped together and assumed proportional to $(\dot{W}_{HE})^2$.

Main Propellant Feed Section

Finite difference techniques were used to simulate the suction and discharge lines to the main engine with representative line lengths chosen for the suction lines. The suction lines (both fuel and liquid oxygen) were represented by symmetrical T-shaped sections and the discharge lines by π-shaped sections. The T-shaped representation of the suction lines allowed explicit expressions to be written for the pump flow rates.

To avoid fuel pump stall during startup and to provide prestart pump cooling, a recirculation valve is located between the pump discharge and fuel tank. Because of the dependence of stall margin and acceleration time on this valve and its associated line, a careful simulation was made. The line was represented by four π-shaped sections, utilizing the aforementioned finite difference techniques. The flow rate through the valve was computed from the following equation:

$$\dot{W}_{RCV} = \left(C_dA\right)_{RCV}\left(2g\rho_F\,\Delta P_{RCV}\right)^{1/2} \tag{25}$$

The fuel pump recirculation valve is spring loaded open and is closed by increased pump discharge pressure as the engine bootstraps.

The thrust chamber valves were similarly treated, when it was assumed that liquid conditions existed at the valves. These valves are initially held closed by spring forces. The opening rate of each valve is a function of its respective pump discharge pressure. Both thrust chamber valves are rigidly connected so that in effect the opening rate of both valves is a function of the average of the two pump discharge pressures (see eqs. (D51) to (D56) in appendix D).

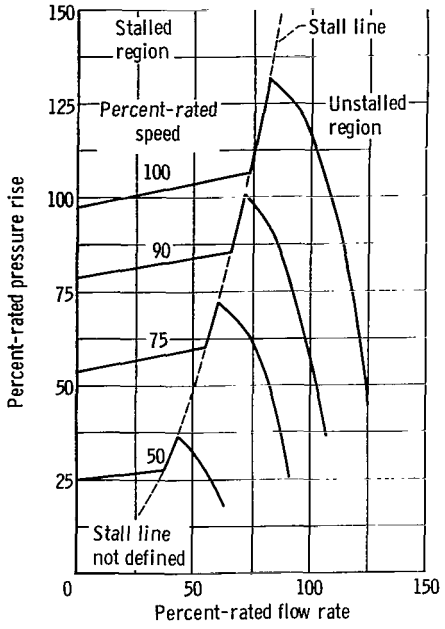

Figure 4. - Estimated pressure rise characteristics for eight-stage axial fuel pump.

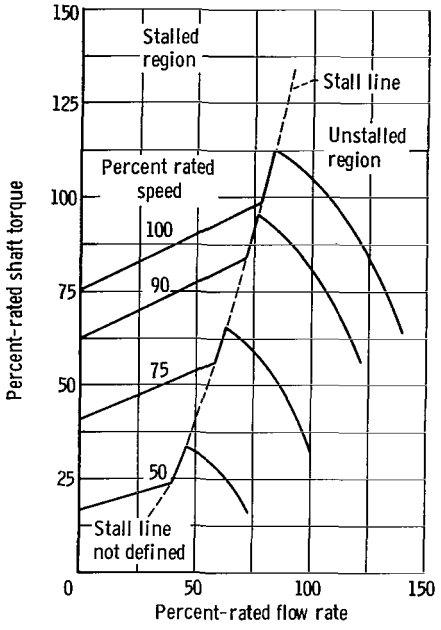

Figure 5. - Estimated torque characteristics for eight-stage axial fuel pump.

The pump characteristics (i. e., pressure rise against pump flow rate and torque against flow rate) supplied by the contractor were represented by curve fits (eqs. (26) to (31)). Pump efficiencies were included in the expressions for pressure rise and torque. The oxidizer pump is a single-stage centrifugal type and the fuel pump is an eight-stage axial design. The fuel pump was represented by two sets of equations. One set was valid for the unstalled region while the other represented the pump while in stall. Only one set of equations was used to represent the oxidizer pump since a large stall margin was expected with the present design. The fuel pump pressure rise and torque characteristics are shown in figures 4 and 5. Transitions between the stalled and unstalled regions were made possible by continuously comparing $\dot{W}/N$ for the fuel pump to the critical value of $\dot{W}/N$, which is characterized by the stall line (figs. 4 and 5). Because of lack of experimental data, the stall line is not defined for speeds less than about 25 percent of nominal. The following equations were used to compute head rise and torque for the two M-1 pumps:

Fuel pump:

Unstalled:

$$\frac{L}{N^2} = K_7 + K_8 \frac{\dot{W}}{N} + K_9 \left(\frac{\dot{W}}{N}\right)^2 \tag{26}$$

$$\frac{\Delta P}{N^2} = K_{10} + K_{11} \frac{\dot{W}}{N} + K_{12} \left(\frac{\dot{W}}{N}\right)^2 + K_{13} \left(\frac{\dot{W}}{N}\right)^3 \tag{27}$$

Stalled:

$$\frac{L}{N^2} = K_{14} + K_{15}\frac{\dot{W}}{N} \tag{28}$$

$$\frac{\Delta P}{N^2} = K_{16} + K_{17}\frac{\dot{W}}{N} \tag{29}$$

Oxidizer pump:

$$\frac{L}{N^2} = K_{18} + K_{19}\frac{\dot{W}}{N} + K_{20}\left(\frac{\dot{W}}{N}\right)^2 \tag{30}$$

$$\frac{\Delta P}{N^2} = K_{21} + K_{22}\frac{\dot{W}}{N} + K_{23}\left(\frac{\dot{W}}{N}\right)^2 \tag{31}$$

The oxidizer pump pressure rise and torque characteristics are presented in figures 6 and 7.

The pressure drop from the thrust chamber valve on the fuel side to the jacket was assumed to be proportional to the square of the flow rate through the valve. The liquid

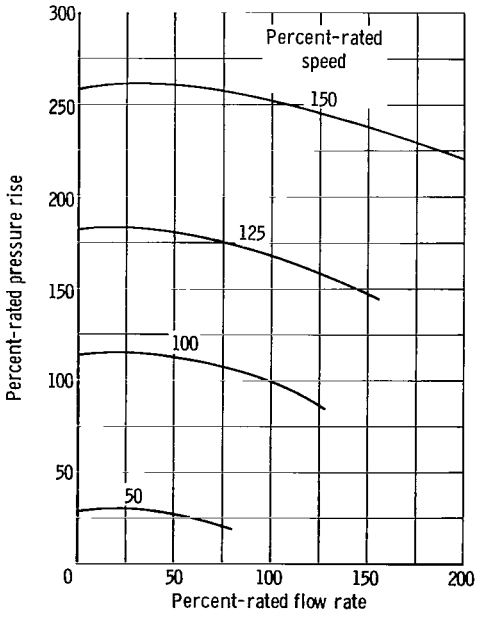

Figure 6. - Estimated pressure rise characteristics for single-stage centrifugal liquid oxygen pump.

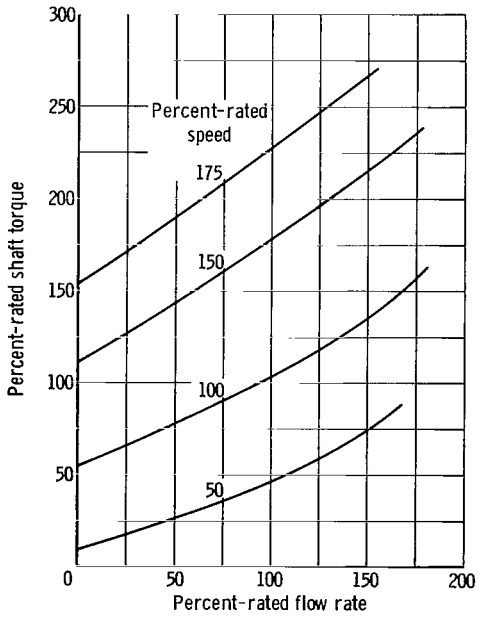

Figure 7. - Estimated torque characteristics for single-stage centrifugal liquid oxygen pump.

oxygen side pressure drop was also assumed to be proportional to the square of the flow rate with the injector drop lumped with the line losses.

Cooling Jacket and Main Engine Assembly

The flow rate through the jacket was assumed to be compressible with heat transfer taking place between the combustion zone and coolant fluid. Based on RL-10 experience, the flow rate was assumed to be proportional to the pressure drop across the jacket (ref. 1).

A one lump finite difference approximation to the jacket was used with the average temperature in the jacket computed from the net heat flow into the fluid. Under the previously mentioned limitation on computing equipment, the following assumptions were made to facilitate the simulation of the cooling jacket (ref. 5): (1) heat flow through the walls was proportional to the temperature difference across the wall; (2) heat flow through the coolant films was proportional to the eight-tenths power of the coolant flow rate; (3) the fuel injector flow rate was computed from equation (25); (4) the average temperature in the jacket $\overline{T}_J$ was equal to the average of the jacket inlet temperature and the fuel injector temperature; and (5) heat transfer between the environment and the outer wall was neglected. Figure 8 shows the one-dimensional model used to represent the cooling jacket. Heat transfer was considered between the combustion zone and coolant tube wall and between the coolant and the coolant tube wall. Axial and circumferential heat transfer within the coolant tube walls, between the inner and outer sections, was neglected. Equations (D73) to (D89) were used to describe the heat-transfer process in the M-1 cooling jacket.

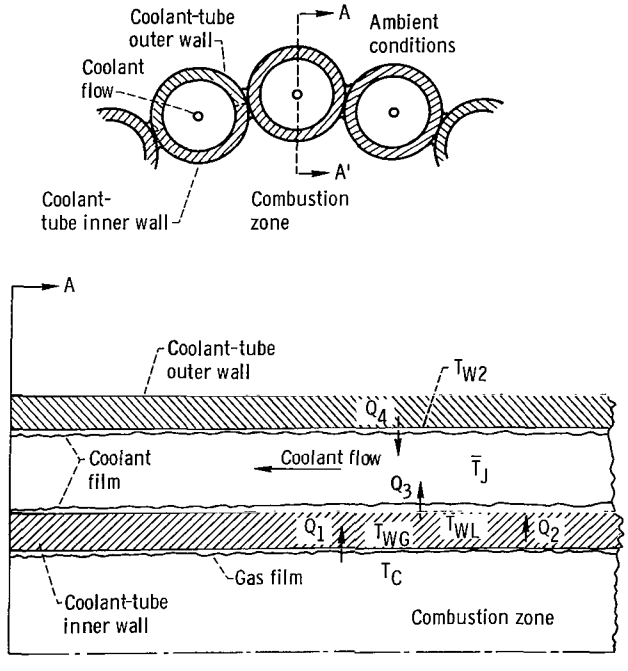

Figure 8. - One-dimensional heat-transfer model for thrust chamber coolant jacket.

The thrust chamber pressure was computed from

$$\tau \frac{dP_C}{dt} + P_C = \frac{C^*}{A_t g} \dot{W}_C \qquad (32)$$

Thrust chamber ignition was delayed until the liquid oxygen injector manifold and its feed line were filled. The filling time was determined by using the same type of pro-

TABLE I. - RESULTS OF AMBIENT PRESSURE STUDY

Ambient back pressure, P_{dsk}, psia	Acceleration time to 90-percent-rated thrust chamber pressure, t_{90}, sec	Thrust chamber ignition time, t_{TC}, sec	Gas generator ignition time, t_{GG}, sec
0	1.49	0.69	0.76
.25	1.52	.68	.77
1.50	1.49	.69	.76
5.00	1.51	.68	.79
14.70	1.60	.75	.82

cedure discussed in connection with the gas generator.

Since this simulation was not intended as a study of combustion instability, combustion delays were not considered in the analysis of the thrust chamber. A summary of all the equations used in this simulation is given in appendix D.

RESULTS AND DISCUSSION

One of the fundamental objectives of the analog program was the determination of the sensitivity of the M-1 start transient to variations in system parameters. To determine the requirements for an altitude start facility, the ambient pressure (back pressure on the extension skirt nozzle) was varied from zero to atmospheric. A trend toward longer start times was noted (table I). Since the data fell within a band of 0.1 second, however, it was decided that it was not necessary to design an altitude start facility solely for the purpose of duplicating a start transient.

The sensitivity of the engine start transient to the fuel pump recirculation configuration was also investigated on the analog computer. This study was made by varying parametrically the recirculation valve area, the spring rate, and the recirculation line diameter and by measuring as performance criteria the time to 90 percent thrust chamber pressure and stall margin. This stall margin is illustrated in figure 9 in which a typical start transient is plotted on a fuel pump map. It is defined as the minimum value of $\frac{\dot{W}}{N} - \left(\frac{\dot{W}}{N}\right)_{stall}$. The selection of $\frac{\dot{W}}{N}$ as the figure of merit is consistent with nondimensional procedures for evaluating pump performance, namely the measurement of Q/ANr, where Q is the volumetric flow rate through the pump. This method avoids the complexities involved in determining pump load lines over a transient range of operation.

Figure 10 shows the effect of the recirculation valve area and line diameter on fuel

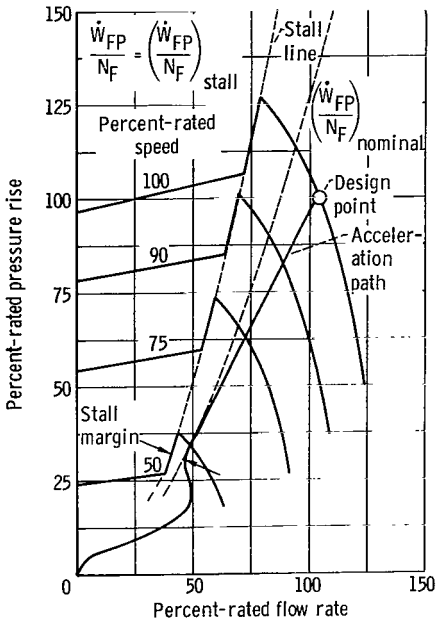

Figure 9. - Typical fuel pump behavior during M-1 start transient.

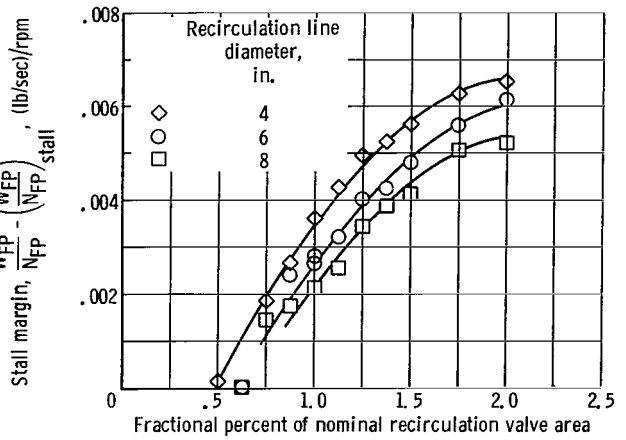

Figure 10. - Effect of recirculation system parameters on fuel pump stall margin. Fixed recirculation spring rate.

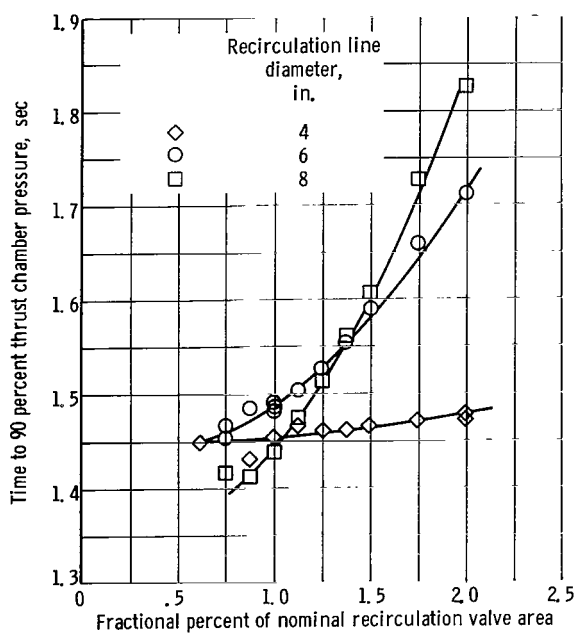

Figure 11. - Effect of recirculation system parameters on acceleration time. All recirculation valve spring rates.

pump stall margin for a fixed (nominal) recirculation valve spring rate. Although increasing the valve flow area resulted in a significant increase in stall margin (stall free accelerations were not possible with valve areas less than 0.6 times nominal), the line diameter had an inverse effect that was possibly caused by the increased inductance of the smaller line. Figure 11 shows the sensitivity of the acceleration time to valve area for 4-, 6-, and 8-inch lines. Since the acceleration time is a minimum and relatively insensitive to valve areas for the 4-inch lines, this is obviously the best choice for rapid, stall-free operation.

Figure 12(a) presents stall margin against recirculation valve flow area for a 4-inch line and various recirculation valve spring rates. Figures 12(b) and (c) present similar data for the 6- and 8-inch lines, respectively. Increasing the spring rate resulted in a significant increase in stall margin for a given line diameter, due to the sustained low flow impedance at the fuel pump discharge. However, the stiffer spring resulted in a decrease in the sensitivity of stall margin to line diameter as shown in figure 13. At 1.2 times the nominal

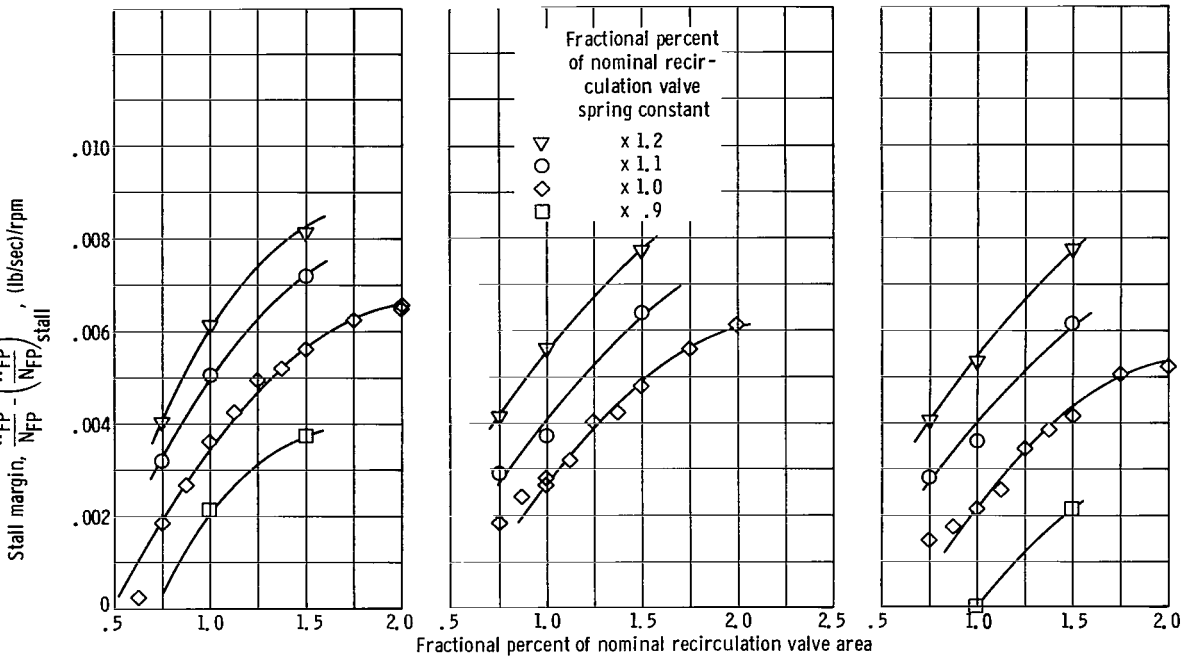

(a) Fixed recirculation line diameter, 4 inches.

(b) Fixed recirculation line diameter, 6 inches.

(c) Fixed recirculation line diameter, 8 inches.

Figure 12. - Effect of recirculation system parameters on fuel pump stall margin.

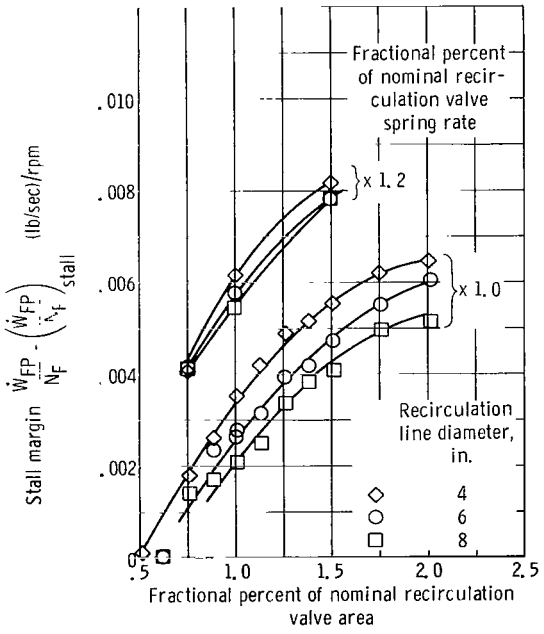

Figure 13. - Effect of recirculation valve spring rate on stall margin sensitivity to line diameter.

spring rate, stall margin is relatively insensitive to line diameter for all valve areas. Acceleration time was found to be insensitive to the recirculation valve spring rate. Therefore, the acceleration time against valve area plot in figure 11 applies for all spring rates. Thus, the best system performance was obtained with the 4-inch line, the recirculation valve area at twice its nominal value, and the recirculation valve spring rate at 1.2 times its nominal value.

To determine the consequences of the failure of the fuel pump recirculation valve to close during startup, the computer model was operated with the valve locked open. Since the valve is initially open and is closed by fuel pump discharge pressure overcoming spring forces on the valve piston, such a failure might occur as a result of a pressure leak at the valve. The results show that the engine bootstrapped to the

TABLE II. - RESULTS OF RECIRCULATION VALVE FAILURE STUDY

Engine parameters	Nominal	Failure
P_c, psi	1040	788
P_{GG}, psi	1145	924
$(O/F)_{TC}$	5.5	9.4
$(O/F)_{GG}$	0.8	1.1

TABLE III. - EFFECT OF SYSTEM VALVE SPRING RATES ON ACCELERATION TIME

Percent of nominal thrust chamber valve spring rate	Percent of nominal gas generator valve spring rate		
	50	100	150
	Acceleration time to 90-percent-rated thrust chamber pressure, t_{90}, sec		
50	----	1.70	----
100	1.38	1.60	2.37
150	1.29	1.50	----

conditions outlined in table II. It is seen that the thrust chamber mixture ratio at these conditions is near stoichiometric. Although the computer model had no burnout limits, and hence, allowed operation in this region, this occurrence on an engine would result in burnout, since this mixture ratio falls outside the design range.

The sensitivity of the engine start transient to the timing (spring rate) of the remaining system valves was also determined. The time to 90-percent thrust chamber pressure was noted for various gas generator and thrust chamber valve spring rates. The significant results are tabulated in table III. Stall margin was not appreciably affected in this study although there was a trend toward longer acceleration times with stiffer gas generator valve springs. This was due to the resulting delay in gas generator ignition and turbopump spinups. The inverse effect of the thrust chamber valve spring rate is due to the increase in flow to the gas generator as the thrust chamber valves are held closed.

To aid in engine-structure coupling studies (POGO), linear transfer functions to represent the M-1 system from the pump inlets to the thrust chamber were determined. The POGO problem results from the coupling of the vehicle structure and engine dynamics in such a way as to produce oscillatory variations in thrust that can be very damaging for both manned and unmanned payloads. Determinations of engine transfer functions early in the development cycle expedite the solution of the problem since it aids in defining the parameters of interest and provides important design data. The transfer functions of interest were the ratios of thrust chamber pressure to propellant tank pressures, assuming sinusoidal pressure perturbations. When the suction lines were removed and the propellant tanks were essentially placed at the pump inlets, results were obtained that would be applicable, regardless of the inlet line dynamics encountered.

Figures 14 and 15 show the magnitude and phase of the transfer function between thrust chamber pressure and oxidizer pump inlet pressure against frequency. Below 20 cps, the magnitude of the transfer function is approximately constant. Figures 16 and and 17 show the magnitude and phase of the liquid oxygen side input impedance against

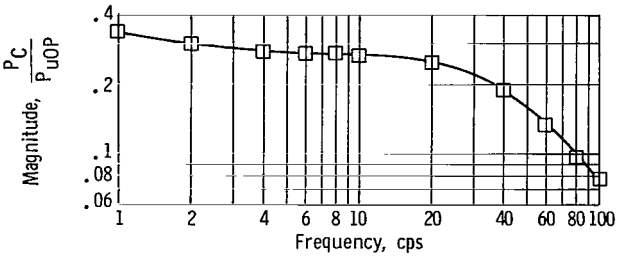

Figure 14. - Magnitude of liquid oxygen side transfer function between thrust chamber pressure and liquid oxygen pump inlet pressure.

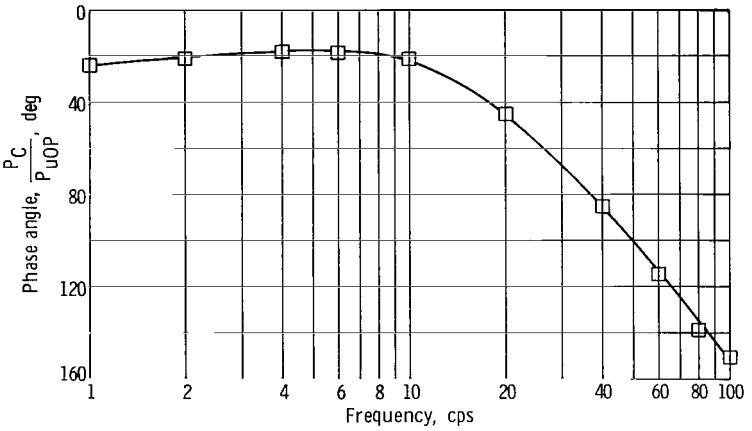

Figure 15. - Phase angle of liquid oxygen side transfer function between thrust chamber pressure and liquid oxygen pump inlet pressure.

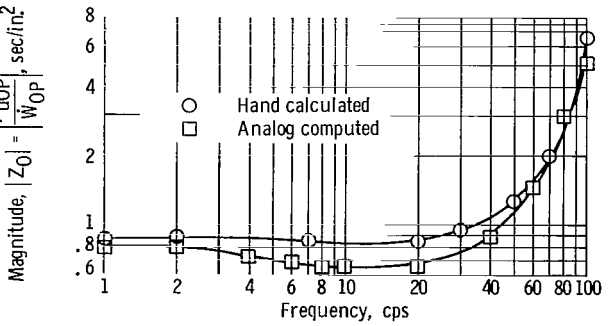

Figure 16. - Magnitude of liquid oxygen input impedance against frequency for analog-computed and hand-calculated cases.

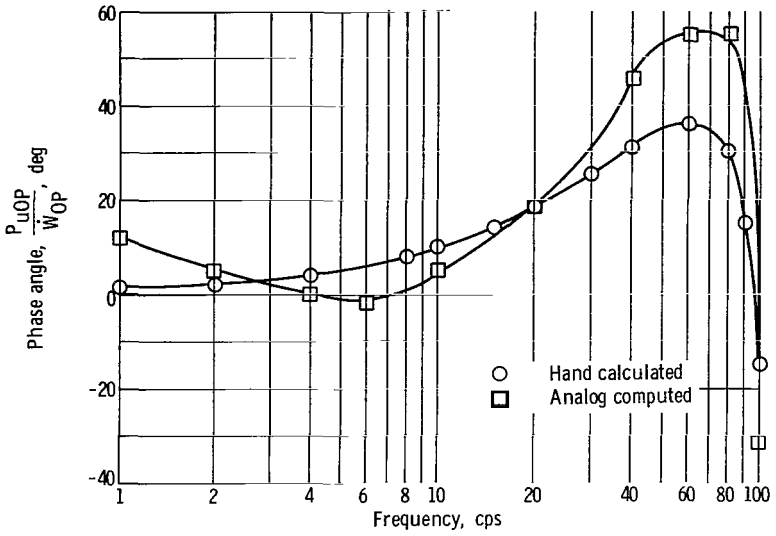

Figure 17. - Phase angle of liquid oxygen input impedance against frequency for analog-computed and hand-calculated cases.

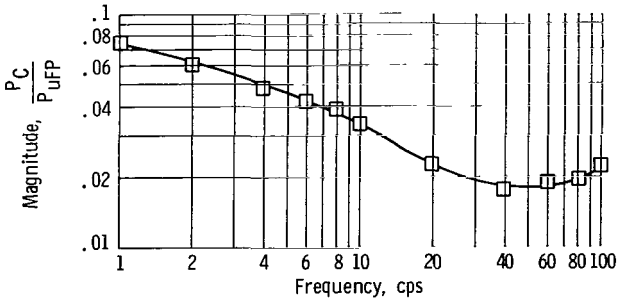

Figure 18. - Magnitude of fuel side transfer function between thrust chamber pressure and fuel pump inlet pressure.

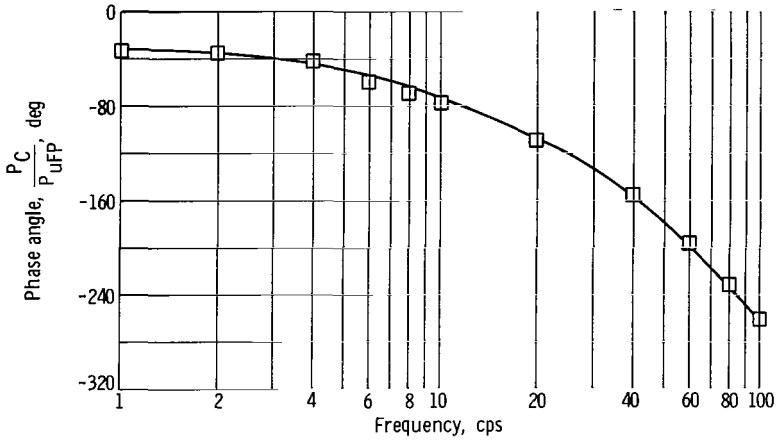

Figure 19. - Phase angle of fuel side transfer function between thrust chamber pressure and fuel pump inlet pressure.

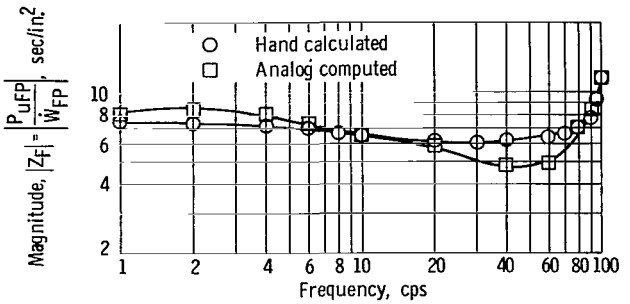

Figure 20. - Magnitude of fuel input impedance against frequency for analog-computed and hand-calculated cases.

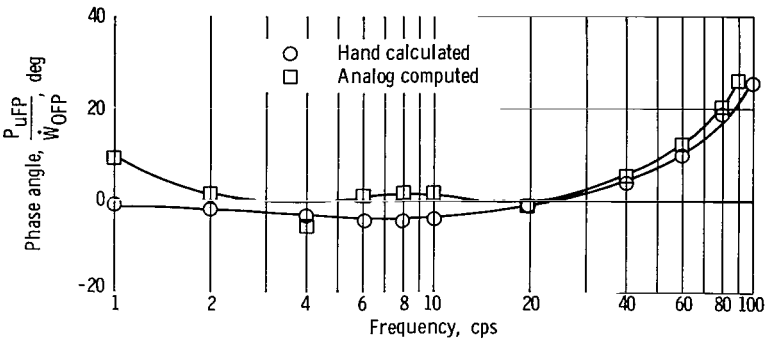

Figure 21. - Phase angle of fuel input impedance against frequency for analog-computed and hand-calculated cases.

frequency. This impedance is defined as the ratio of pump inlet pressure to pump flow rate. The effect of cavitation bubbles on the inlet impedance was neglected. As in the case of the pressure/pressure transfer function, frequency effects were small below 20 cps. To support the analog results, hand calculations of the input impedance were made and the results of these calculations are also plotted in figures 16 and 17. The hand analysis is described in detail in appendix E.

Figures 18 and 19 show the magnitude and phase of the transfer function between thrust chamber pressure and fuel pump inlet pressure. As in the case of the liquid oxygen side, both computer and hand calculated results were obtained for the fuel flow impedance Z_F and are presented in figures 20 and 21. For frequencies below 50 cps, the fuel impedance can be approximated by a constant that is independent of frequency. The desired transfer functions between thrust chamber pressure and propellant tank pressures can be obtained, for any given suction line impedance, by using the following equations:

$$\frac{P_C}{P_{TO}} = \left(\frac{P_C}{P_{uOP}}\right)\left(\frac{Z_O}{Z_O + Z_{SO}}\right) \tag{33}$$

where Z_{SO} is the impedance of oxidant suction line and

$$\frac{P_C}{P_{TF}} = \left(\frac{P_C}{P_{uFP}}\right)\left(\frac{Z_F}{Z_F + Z_{SF}}\right) \tag{34}$$

where Z_{SF} is the impedance of fuel suction line.

Since no combustion dead time was considered in the analysis, it should be noted that the addition of an estimated 0.7 millisecond dead time (ref. 6) to the engine dynamics would contribute a maximum of about 30° to the input impedance characteristics at 100 cps.

CONCLUSIONS

The analog computer simulation of the M-1 rocket engine system yielded the following information concerning engine characteristics:

1. The effect of ambient pressure on the engine start transient was found to be negligible with pressures ranging from zero to atmospheric (the figures of merit being fuel pump stall margin and the time to reach 90-percent thrust chamber pressure).

2. Stall margin could, in general, be increased by increasing the recirculation valve area at the cost of increased acceleration time. Stall margin was found to be a slight inverse function of recirculation line diameter. A decrease in acceleration time, together with an increase in stall margin, was obtained by using the 4-inch line with recirculation valve areas and spring rates greater than nominal.

3. Failure of the recirculation valve to close during the start would result in a steady-state thrust chamber mixture ratio near stoichiometric, with a resulting burnout of the thrust chamber.

4. Thrust chamber to propellant tank pressure ratios can be obtained from engine impedance characteristics measured on the analog computer. Over the range of expected POGO oscillations (0 to 20 cps), the engine impedance characteristics may be assumed constant with the dominant dynamics expected from the inlet lines.

Lewis Research Center,
National Aeronautics and Space Administration,
Cleveland, Ohio, August 11, 1965.

APPENDIX A

SYMBOLS

A	cross-sectional area, throat area, $in.^2$
B	fluid bulk modulus, $lb/in.^2$
C	fluid capacitance, $in.^2$
C_D	orifice discharge coefficient
C^*	characteristic exhaust velocity (function of chamber mixture ratio), in./sec
c	isentropic spouting velocity, in./sec
c_p	specific heat of fluid at constant pressure, $Btu/(lb)(^oR)$
F	flow correction factor to account for variations in fluid properties
f_i	general functional relation (i = integer)
g	gravitational constant, $in./sec^2$
h	specific enthalpy, Btu/lb
Δh	specific enthalpy drop (assumed positive) across turbine, Btu/lb
I	turbopump moment of inertia, $in.-lb/sec^2$
J	mechanical heat equivalent (constant), in.-lb/Btu
K_i	proportionality constants (i = integer), appropriate dimensions
K_r	rated turbine static to total discharge pressure ratio
L	shaft torque, in.-lb
$\mathscr{l}$	hydraulic line inductance, $sec^2/in.^2$
l	length, in.
M	Mach number
N	turbopump shaft rotational speed, rpm
O/F	oxidant fuel ratio
P	absolute total pressure, $lb/in.^2$
ΔP	absolute total pressure change (assumed positive), $lb/in.^2$
p	absolute static pressure, $lb/in.^2$
Q	volumetric flow rate, $in.^3/sec$
q	rate of heat flow, Btu/sec
R	universal gas constant, $in./^oR$
$\mathscr{R}$	hydraulic flow resistance, appropriate dimension
r	mean turbine blade radius, in.
S	Laplace operator, 1/sec
T	total temperature, ^oR
t	time measured from start, sec
u	turbine bucket mean peripheral velocity, in./sec
V	plenum volume, $in.^3$
$\dot{W}$	rate of fluid weight flow, lb/sec

χ	general fluid property, appropriate dimension
y	valve stroke, in.
Z	flow impedance, sec/in.^{2}
β	percent burnt products in turbine driving gases
γ	fluid specific heat ratio
η	efficiency, $(0 \leq \eta \leq 1.0)$
ρ	fluid density (constant unless otherwise specified), lb/in.^{3}
τ	chamber relaxation time, sec

Subscripts:

ACT	actual valve
BP	gas generator burnt products
C	thrust chamber
D	pump discharge
d	downstream
F	fuel
FP	fuel pump
FT	fuel turbine
GG	gas generator
HE	helium
ID	ideal value
IL	interstage line
INJ	injector
i	initial value
J	coolant jacket
J1	upstream half of coolant jacket
J2	downstream half of coolant jacket
M	helium - O/F mixture
man	manifold
O	oxidant
ORF	engine balance orifice
OT	oxidant turbine
P	pump (in general)
PA	piston actuating
PUV	propellant utilization valve
RC	recirculation
r	at rated mixture ratio
SF	fuel suction line
SK	nozzle extension skirt
SO	oxidant suction line
SV	start valve
T	tank
TAP	main line tapoff
TC	thrust chamber
TUR	turbine (general)
t	throat
u	upstream
V	valve
WG	coolant tube wall (combustion zone side)
WL	coolant tube wall (coolant flow side)
W_2	coolant tube wall (ambient side)

Superscript:

–	average

APPENDIX B

TIME AND VOLTAGE SCALING

Since the computers used are 100-volt devices, all system variables must be scaled so as not to exceed that value. The voltage representing any variable α is designated E_α and is related to α by the expression $E_\alpha = \alpha/SF$ where SF is the voltage scale factor. To facilitate data recording and the use of servodriven multipliers, the problem was slowed down (time-scaled) by a factor of 100.

Hot Gas and Helium Section

General parameter, α	Scale factor, SF	Maximum general parameter, α_{max}
y_{GGO}	0.015	1.5
$\dot{W}_{GGO}$	.8	80
$\dot{W}_{GGF}$	1	100
$\dot{W}$ (all others)	1.5	150
P_{GG}	12	1200
P_{uFT}	12	1200
P_{dFT}	5	500
P_{uOT}	5	500
P_{dOT}	2	200
P_{HE}	50	5000
P_{dSV}	50	5000
p_d/P_u (all)	.01	1
R (all)	8	800
T_{HE}	4	400
T (all others)	40	4000
c_P (all)	.04	4
$(\Delta h_{ACT})_F$	8	800
$(\Delta h_{ID})_F$	10	1000
$(\Delta h_{ACT})_O$	2	200
$(\Delta h_{ID})_O$	4	400

β	0.01	1
η (all)	.01	1
u_F	30	3 000
u_O	5	500
c_F	100	10 000
c_O	100	10 000
N_O	40	4 000
N_F	150	15 000
L_{OT}	400	40 000
L_{FT}	400	40 000

Main Line and Pump Section

General parameter, α	Scale factor, SF	Maximum general parameter, α_{max}
$\dot{W}_O$ (all flows)	40	4 000
$\dot{W}_F$ (all flows)	8	800
P_{TO}	1	100
P_{TF}	1	100
P_O (all others)	20	2 000
P_F (all others)	25	2 500
L_{OP}	400	40 000
L_{FP}	400	40 000

Cooling Jacket and Main Engine

General parameter, α	Scale factor, SF	Maximum general parameter, α_{max}
T_C	75	7 500
T_{WG}	30	3 000
T_{WL}	30	3 000
T_{W2}	6	600
T_F	1	100

$\overline{T}_J$	2.5	2 500
T_{INJ}	3	300
q (all)	2500	250 000
$\dot{W}_O$ (all)	40	4 000
$\dot{W}_F$ (all)	8	800
$\dot{W}_C$	40	4 000
P_O (all)	20	2 000
P_F (all)	25	2 500
P_C	12.5	1 250

APPENDIX C

MIXING OF HELIUM AND GAS GENERATOR BURNT PRODUCTS

To account for variations in fluid properties due to the mixing of helium and gas generator burnt products, it is necessary to derive c_p, R, and h for the mixture, assuming perfect instantaneous mixing in a plenum. The following definitions are used:

W_1	weight of fluid 1 in plenum
W_2	weight of fluid 2 in plenum
$\dot{W}_1$	rate of flow of fluid 1 into plenum
$\dot{W}_2$	rate of flow of fluid 2 into plenum
C_{p1}	specific heat of fluid 1
C_{p2}	specific heat of fluid 2
R_1	gas constant of fluid 1
R_2	gas constant of fluid 2
h_1	specific enthalpy of fluid 1
h_2	specific enthalpy of fluid 2
M	subscript denoting desired mixture properties
χ	general fluid property (either C_p, R, h)

Then

$$\chi_M = \frac{W_1\chi_1 + W_2\chi_2}{W_1 + W_2} = \frac{\int \chi_1\dot{W}_1\,dt + \int \chi_2\dot{W}_2\,dt}{\int (W_1 + W_2)dt}$$

Cross multiplying yields

$$\chi_M \int (\dot{W}_1 + \dot{W}_2)dt = \int \chi_1\dot{W}_1\,dt + \int \chi_2\dot{W}_2\,dt$$

When it is assumed that χ_1 and χ_2 do not vary appreciably during the mixing process,

$$\chi_M \int (\dot{W}_1 + \dot{W}_2)dt = \chi_1 \int \dot{W}_1\,dt + \chi_2 \int \dot{W}_2\,dt$$

By differentiating both sides with respect to time, we get

$$\chi_M(\dot{W}_1 + \dot{W}_2) = \chi_1\dot{W}_1 = \chi_2\dot{W}_2$$

Therefore,

$$\chi_M = \chi_1 \frac{\dot{W}_1}{\dot{W}_1 + \dot{W}_2} + \chi_2 \frac{\dot{W}_2}{\dot{W}_1 + \dot{W}_2}$$

$$\chi_M = \beta\chi_1 + (1 - \beta)\chi_2$$

where β is the percent of fluid 1 in the resulting mixture.

The preceding derivation is based on the assumption that mixing takes place instantaneously in a small plenum. The result may be modified to more closely represent the physical process as

$$\tau_M \frac{d\chi_M}{dt} + \chi_M = \beta\chi_1 + (1 - \beta)\chi_2$$

where τ_M is the mixing time constant.

APPENDIX D

EQUATION SUMMARY

Helium and Hot Gas Section

$$y_{GGV} = K_1 \int_0^t P_{dFP}\, dt + K_2 \tag{D1}$$

$$\dot{W}_{GGO} = \left(C_D A\right)_O \left[2g\rho_O \left(\Delta P_{GGV}\right)_O\right]^{1/2} \tag{D2}$$

$$\dot{W}_{GGF} = \left(C_D A\right)_F \left[2g\rho_F \left(\Delta P_{GGV}\right)_F\right]^{1/2} \tag{D3}$$

$$A_O = f_1(y_{GGV}) \tag{D4}$$

$$A_F = f_2(y_{GGV}) \tag{D5}$$

$$\dot{W}_{ORF} = \left(C_D A\right)_{ORF} \left(2g\rho_{ORF}\, \Delta P_{ORF}\right)^{1/2} \tag{D6}$$

$$\rho_{ORF} = \frac{P_{GG} + P_{uFT}}{2R_M T_M} \tag{D7}$$

$$\dot{W}_{FT} = \frac{P_{uFT} A_{FT}}{\left(R_M T_M\right)^{1/2}} \left(K_{rF} \frac{P_{dFT}}{P_{uFT}}\right)^{1/\gamma_r} \left[K_3 \left(\frac{\gamma_M - 1}{\gamma_M}\right) + K_4\right]$$

$$\times \left\{\frac{2g\gamma_r}{\gamma_r - 1}\left[1 - \left(K_{rF} \frac{P_{dFT}}{P_{uFT}}\right)^{(\gamma_r - 1)/\gamma_r}\right]\right\}^{1/2} \tag{D8}$$

$$\dot{W}_{OT} = \frac{P_{uOT}A_{OT}}{(R_M T_{uOT})^{1/2}} \left(K_{rO} \frac{P_{dOT}}{P_{uOT}}\right)^{1/\gamma_r} \left[K_3\left(\frac{\gamma_M - 1}{\gamma_M}\right) + K_4\right]$$

$$\times \left\{\frac{2g\gamma_r}{\gamma_r - 1}\left[1 - \left(K_{rO}\frac{P_{dOT}}{P_{uOT}}\right)^{(\gamma_r - 1)/\gamma_r}\right]\right\}^{1/2} \tag{D9}$$

$$\frac{\gamma_M - 1}{\gamma_M} = 8.03\times10^{-4}\,\frac{R_M}{C_{PM}} \tag{D10}$$

$$\dot{W}_{PuV} = \frac{A_{PuV}\dot{W}_{FT}}{A_{FT}} \tag{D11}$$

$$\dot{W}_{IL} = \frac{1}{\ell_{IL}} \int_0^t \left(P_{dFT} - P_{uOT} - \rho_{IL}\dot{W}_{IL}^2\right)dt \tag{D12}$$

$$\dot{W}_{SK} = \frac{A_{SK}P_{dOT}}{(R_M T_{dOT})^{1/2}} \left(\frac{2}{\gamma_M + 1}\right)^{1/(\gamma_M - 1)} \left(\frac{2g\gamma_M}{\gamma_M + 1}\right)^{1/2} \tag{D13}$$

$$\dot{W}_{HE} = \frac{P_{HE}A_{SV}}{(R_{HE}T_{HE})^{1/2}} \left(\frac{P_{dSV}}{P_{HE}}\right)^{1/\gamma_{HE}} \left\{\frac{2g\gamma_{HE}}{\gamma_{HE} - 1}\left[1 - \left(\frac{P_{dSV}}{P_{HE}}\right)^{(\gamma_{HE} - 1)/\gamma_{HE}}\right]\right\}^{1/2} \tag{D14}$$

$$\Delta P_{ORF} = P_{GG} - P_{uFT} \tag{D15}$$

$$\left(\Delta P_{GGV}\right)_O = P_{TAPO} - P_{GG} \tag{D16}$$

$$\left(\Delta P_{GGV}\right)_F = P_{TAPF} - P_{GG} \tag{D17}$$

$$P_{GG} = \frac{R_{BP}T_{GG}}{V_{GG}} \int_0^t \left(\dot{W}_{GGO} + \dot{W}_{GGF} - \dot{W}_{ORF}\right)dt \tag{D18}$$

$$P_{uFT} = \frac{R_M T_M}{V_{uFT}} \int_0^t (\dot{W}_{ORF} + \dot{W}_{HE} - \dot{W}_{FT} - \dot{W}_{PuV})dt \tag{D19}$$

$$P_{dFT} = \frac{R_M T_{uOT}}{\frac{1}{2} V_{IL}} \int_0^t (\dot{W}_{FT} + \dot{W}_{PuV} - \dot{W}_{IL})dt \tag{D20}$$

$$P_{uOT} = \frac{R_M T_{uOT}}{\frac{1}{2} V_{IL}} \int_0^t (\dot{W}_{IL} - \dot{W}_{OT})dt \tag{D21}$$

$$P_{dOT} = \frac{R_M T_{dOT}}{V_{dOT}} \int_0^t (\dot{W}_{OT} - \dot{W}_{SK})dt \tag{D22}$$

$$P_{dSV} = P_{uFT} + \rho_{SV} \dot{W}_{HE}^2 \tag{D23}$$

$$\left(\Delta h_{ID}\right)_F = C_{PM} T_M \left[1 - \left(K_{rF} \frac{P_{dFT}}{P_{uOT}}\right)^{(\gamma_M - 1)/\gamma_M}\right] \tag{D24}$$

$$\left(\Delta h_{ID}\right)_O = C_{PM} T_{uOT} \left[1 - \left(K_{rO} \frac{P_{dOT}}{P_{uOT}}\right)^{(\gamma_M - 1)/\gamma_M}\right] \tag{D25}$$

$$\left(\Delta h_{ACT}\right)_F = \eta_{FT} \left(\Delta h_{ID}\right)_F \tag{D26}$$

$$\left(\Delta h_{ACT}\right)_O = \eta_{OT} \left(\Delta h_{ID}\right)_O \tag{D27}$$

$$\eta_{FT} = K_5 \left(\frac{u}{c}\right)_F + K_6 \left(\frac{u}{c}\right)_F^2 \tag{D28}$$

$$\eta_{OT} = K_5 \left(\frac{u}{c}\right)_O + K_6 \left(\frac{u}{c}\right)_O^2 \tag{D29}$$

$$\mu_O = \frac{\pi r_{OT}}{30} N_O \tag{D30}$$

$$\mu_F = \frac{\pi r_{FT}}{30} N_F \tag{D31}$$

$$c_O = \left[2gJ\left(\Delta h_{ACT}\right)_O\right]^{1/2} \tag{D32}$$

$$c_F = \left[2gJ\left(\Delta h_{ACT}\right)_F\right]^{1/2} \tag{D33}$$

$$L_{OT} = \frac{J}{2\pi} \dot{W}_{OT} \frac{\left(\Delta h_{ACT}\right)_O}{N_O} \tag{D34}$$

$$L_{FT} = \frac{J}{2\pi} \dot{W}_{FT} \frac{\left(\Delta h_{ACT}\right)_F}{N_F} \tag{D35}$$

$$N_O = \frac{30}{\pi I_O} \int_0^t (L_{OT} - L_{OP})dt \tag{D36}$$

$$N_F = \frac{30}{\pi I_F} \int_0^t (L_{FT} - L_{FP})dt \tag{D37}$$

$$T_{uOT} = T_M - \frac{1}{c_{PM}} \left[\frac{\dot{W}_{FT}\left(\Delta h_{ACT}\right)_F}{\dot{W}_{FT} + \dot{W}_{PuV}}\right] \tag{D38}$$

$$T_{dOT} = T_{uOT} - \frac{\left(\Delta h_{ACT}\right)_O}{c_{PM}} \tag{D39}$$

$$\beta = \frac{\dot{W}_{GGO} + \dot{W}_{GGF}}{\dot{W}_{GGO} + \dot{W}_{GGF} + \dot{W}_{HE}} \tag{D40}$$

$$c_{PM} = \beta c_{pBP} + (1 - \beta)c_{pHE} \tag{D41}$$

$$R_M = \beta R_{BP} + (1 - \beta)R_{HE} \tag{D42}$$

$$c_{PM}T_M = \beta c_{pBP}T_{BP} + (1 - \beta)c_{pHE}T_{HE} \tag{D43}$$

$$T_{HE}P_{HE}^{1-\gamma_{HE}/\gamma_{HE}} = T_iP_i^{1-\gamma_{HE}/\gamma_{HE}} \tag{D44}$$

Main Line and Pump Section

$$\dot{W}_{SO} = \frac{2}{\ell_{SO}} \int_0^t \left(P_{TO} - P_{SO} - \frac{R_{SO}}{2}\dot{W}_{SO}^2\right)dt \tag{D45}$$

$$\dot{W}_{SF} = \frac{2}{\ell_{SF}} \int_0^t \left(P_{TF} - P_{SF} - \frac{R_{SF}}{2}\dot{W}_{SF}^2\right)dt \tag{D46}$$

$$\dot{W}_{OP} = \frac{2}{\ell_{SO}} \int_0^t \left(P_{SO} - P_{dOP} + \Delta P_{OP} - \frac{R_{SO}}{2}\dot{W}_{OP}^2\right)dt \tag{D47}$$

$$\dot{W}_{FP} = \frac{2}{\ell_{SF}} \int_0^t \left(P_{SF} - P_{dFP} + \Delta P_{FP} - \frac{R_{SF}}{2}\dot{W}_{FP}^2\right)dt \tag{D48}$$

$$\dot{W}_{DO} = \frac{1}{\ell_{DO}} \int_0^t \left(P_{dOP} - P_{TAPO} - R_{DO}\dot{W}_{DO}^2\right)dt \tag{D49}$$

$$\dot{W}_{DF} = \frac{1}{\ell_{DF}} \int_0^t \left(P_{dFP} - P_{TAPF} - R_{DF}\dot{W}_{DF}^2\right)dt \tag{D50}$$

$$\left(\dot{W}_{TCV}\right)_O = \left(C_DA_{TCV}\right)_O\left[2g\rho_O\left(\Delta P_{TCV}\right)_O\right]^{1/2} \tag{D51}$$

$$\left(\dot{W}_{TCV}\right)_F = \left(C_D A_{TCV}\right)_F \left[2g\rho_F \left(\Delta P_{TCV}\right)_F\right]^{1/2} \tag{D52}$$

$$\dot{W}_{RCV} = \left(C_D A\right)_{RCV} \left(2g\rho_F \, \Delta P_{RCV}\right)^{1/2} \tag{D53}$$

$$A_{TCVO} = f_3(P_{dOP} + P_{dFP}) \tag{D54}$$

$$A_{TCVF} = f_4(P_{dOP} + P_{dFP}) \tag{D55}$$

$$A_{RCV} = f_5(P_{dFP}) \tag{D56}$$

$$\left(\frac{L_{FP}}{N_F^2}\right)_{\text{unstalled}} = K_7 + K_8\left(\frac{\dot{W}_{FP}}{N_F}\right) + K_9\left(\frac{\dot{W}_{FP}}{N_F}\right)^2 \tag{D57}$$

$$\left(\frac{\Delta P_{FP}}{N_F^2}\right)_{\text{unstalled}} = K_{10} + K_{11}\left(\frac{\dot{W}_{FP}}{N_F}\right) + K_{12}\left(\frac{\dot{W}_{FP}}{N_F}\right)^2 + K_{13}\left(\frac{\dot{W}_{FP}}{N_F}\right)^3 \tag{D58}$$

$$\left(\frac{L_{FP}}{N_F^2}\right)_{\text{stalled}} = K_{14} + K_{15}\left(\frac{\dot{W}_{FP}}{N_F}\right) \tag{D59}$$

$$\left(\frac{\Delta P_{FP}}{N_F^2}\right)_{\text{stalled}} = K_{16} + K_{17}\left(\frac{\dot{W}_{FP}}{N_F}\right) \tag{D60}$$

$$\frac{L_{OP}}{N_O^2} = K_{18} + K_{19}\left(\frac{\dot{W}_{OP}}{N_O}\right) + K_{20}\left(\frac{\dot{W}_{OP}}{N_O}\right)^2 \tag{D61}$$

$$\frac{\Delta P_{OP}}{N_O^2} = K_{21} + K_{22}\left(\frac{\dot{W}_{OP}}{N_O}\right) + K_{23}\left(\frac{\dot{W}_{OP}}{N_O}\right)^2 \tag{D62}$$

$$P_{SO} = \frac{B_O}{\rho_O V_{SO}} \int_0^t (\dot{W}_{SO} - \dot{W}_{OP})dt \tag{D63}$$

$$P_{SF} = \frac{B_F}{\rho_F V_{SF}} \int_0^t (\dot{W}_{SF} - \dot{W}_{FP})dt \tag{D64}$$

$$P_{dOP} = \frac{2B_O}{\rho_O V_{DO}} \int_0^t (\dot{W}_{OP} - \dot{W}_{DO})dt \tag{D65}$$

$$P_{dFP} = \frac{2B_F}{\rho_F V_{DF}} \int_0^t (\dot{W}_{FP} - \dot{W}_{DF})dt \tag{D66}$$

$$P_{TAPO} = \frac{2B_O}{\rho_O V_{DO}} \int_0^t \left[\dot{W}_{DO} - \dot{W}_{GGO} - \left(\dot{W}_{TCV}\right)_O\right]dt \tag{D67}$$

$$P_{TAPF} = \frac{2B_F}{\rho_F V_{DF}} \int_0^t \left[\dot{W}_{DF} - \dot{W}_{GGF} - \left(\dot{W}_{TCV}\right)_F\right]dt \tag{D68}$$

$$P_{uJ} = P_J + \frac{R_J}{2}\dot{W}_{J1} \tag{D69}$$

$$\left(\Delta P_{TCV}\right)_O = P_{TAPO} - \left(P_{INJ}\right)_O \tag{D70}$$

$$\left(\Delta P_{TCV}\right)_F = P_{TAPF} - P_{uJ} \tag{D71}$$

$$\Delta P_{RCV} = P_{dFP} - P_{TF} \tag{D72}$$

Cooling Jacket and Main Engine (see fig. 7)

$$q_1 = K_{24}(\dot{W}_C)^{0.8}(T_C - T_{WG}) \tag{D73}$$

$$q_2 = K_{25}(T_{WG} - T_{WL}) \tag{D74}$$

$$q_3 = K_{26}\left(\dot{W}_{TCV}\right)_F^{0.8}(T_{WL} - \overline{T}_J) \tag{D75}$$

$$q_4 = K_{27}\left(\dot{W}_{TCV}\right)_F^{0.8}(T_{W2} - \overline{T}_J) \tag{D76}$$

$$T_{WG} = K_{28}\int_0^t (q_1 - q_2)dt \tag{D77}$$

$$T_{WL} = K_{29}\int_0^t (q_2 - q_3)dt \tag{D78}$$

$$T_{W2} = K_{30}\int_0^t q_4\, dt \tag{D79}$$

$$\overline{T}_J = K_{31}\frac{q_3 + q_4}{\left(\dot{W}_{TCV}\right)_F} + T_F \tag{D80}$$

$$\left(T_{INJ}\right)_F = 2\overline{T}_J - T_F \tag{D81}$$

$$\left(\dot{W}_{INJ}\right)_O = \left(\dot{W}_{TCV}\right)_O \tag{D82}$$

$$\dot{W}_{J1} = \left(\dot{W}_{TCV}\right)_F \tag{D83}$$

$$\dot{W}_{J2} = \frac{2}{\rho_J}\left[P_J - \left(P_{INJ}\right)_F\right] \tag{D84}$$

$$\left(\dot{W}_{INJ}\right)_F = K_{32}\left\{\frac{\left[P_C + \left(P_{INJ}\right)_F\right]\left[\left(P_{INJ}\right)_F - P_C\right]}{T_{INJ}}\right\}^{1/2} \tag{D85}$$

$$\dot{W}_C = \left(\dot{W}_{INJ}\right)_O + \left(\dot{W}_{INJ}\right)_F \tag{D86}$$

$$\left(P_{INJ}\right)_O = \left(\rho_{INJ}\right)_O \left(\dot{W}_{INJ}\right)_O^2 + P_C \tag{D87}$$

$$P_J = \frac{R_F \overline{T}_J}{V_J} \int_0^t (\dot{W}_{J1} - \dot{W}_{J2})dt \tag{D88}$$

$$\left(P_{INJ}\right)_F = \frac{R_F \left(T_{INJ}\right)_F}{\left(V_{INJ}\right)_F} \int_0^t \left(\dot{W}_{J2} - \dot{W}_{INJ}\right)_F dt \tag{D89}$$

$$\frac{\tau dP_C}{dt} + P_C = \frac{C^*}{A_C g} \dot{W}_C \tag{D90}$$

$$C^* = f_6\left(\frac{\dot{W}_{INJO}}{\dot{W}_{INJF}}\right) \tag{D91}$$

APPENDIX E

CALCULATION OF M-1 OXIDIZER FLOW IMPEDANCE

To aid in engine-vehicle coupling studies (POGO), it is necessary to obtain thrust to propellant tank pressure frequency response data. A primary step in obtaining this information is the calculation of flow impedances ($Z_O = \partial P_{uOP}/\partial \dot{W}_{OP}$) for the various segments of the M-1 system. The segment considered in this analysis is illustrated in figure 22. When standard perturbation techniques and the design values for flow rates and pressures are used, the electrical analog to the fluid system shown in figure 23 can be obtained. One π-shaped section was used to approximate the discharge line. All pressures and flows represent perturbations from the operating point. The values computed for the system parameters are shown in table IV. These values, together with classical circuit reduction techniques, allowed us to obtain the following expression for the oxidant impedance Z_O:

$$Z_O = \frac{K_{33}S^4 + K_{34}S^3 + K_{35}S^2 + K_{36}S + K_{37}}{K_{38}S^4 + K_{39}S^3 + K_{40}S^2 + K_{41}S + K_{42}}$$

where

$K_{33} = 7.1\times10^{-13}$ $\quad K_{37} = 2.92$ $\quad K_{40} = 1.17\times10^{-5}$

$K_{34} = 6.79\times10^{-9}$ $\quad K_{38} = 2.85\times10^{-12}$ $\quad K_{41} = 7.35\times10^{-3}$

$K_{35} = 1.64\times10^{-5}$ $\quad K_{39} = 1.51\times10^{-8}$ $\quad K_{42} = 3.43$

$K_{36} = 1.42\times10^{-2}$

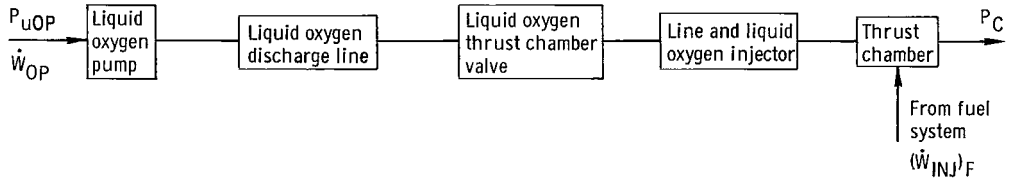

Figure 22. - Block diagram of M-1 oxidizer system.

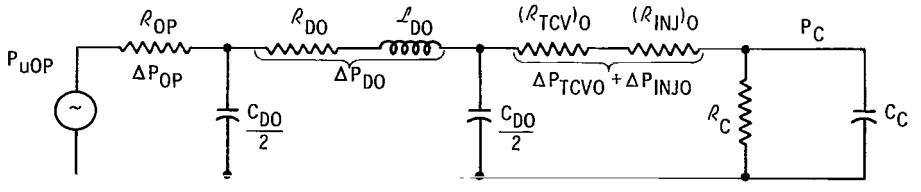

Figure 23. - Electrical analog representation of M-1 oxidizer system.

TABLE IV. - SYSTEM PARAMETER VALUES

System parameters		Computed values
Definition	Equation	
Liquid oxygen pump flow resistance, sec/in.^{2}	$R_{OP} = \frac{\partial \Delta\bar{P}_{OP}}{\partial \dot{W}_{OP}}$	0.25
Liquid oxygen discharge line flow resistance, sec/in.^{2}	$R_{DX} = \frac{\partial \Delta\bar{P}_{DO}}{\partial \dot{W}_{DO}}$	1.15×10^{-2}
Liquid oxygen thrust chamber valve flow resistance, sec/in.^{2}	$R_{TCVO} = \frac{\partial \Delta\bar{P}_{TCVO}}{\partial \dot{W}_{TCVO}}$	3.54×10^{-2}
Thrust chamber flow resistance, sec/in.^{2}	$R_C = \frac{\partial \bar{P}_C}{\partial \dot{W}_{TCVO}}$	0.292
Liquid oxygen injector flow resistance, sec/in.^{2}	$R_{INJO} = \frac{\partial \Delta P_{INJO}}{\partial \dot{W}_{TCVO}}$	0.276
Liquid oxygen discharge line inductance, sec^2/in.^{2}	$\mathcal{L}_{DO} = \frac{l_{DO}}{A_{DO} g}$	2.96×10^{-3}
Fluid capacitance of discharge line, in.^{2}	$C_{DO} = \frac{\rho_O V_{DO}}{B_O}$	1.9×10^{-3}
Fluid capacitance of thrust chamber, in.^{2}	$C_C = \frac{\tau}{R_C}$	3.43×10^{-3}

A similar procedure was followed to determine the impedance for the fuel system when heat transfer in the jacket was neglected. The resultant flow impedance was

$$Z_F = \frac{K_{43}S^6 + K_{44}S^5 + K_{45}S^4 + K_{46}S^3 + K_{47}S^2 + K_{48}S + K_{49}}{K_{50}S^6 + K_{51}S^5 + K_{52}S^4 + K_{53}S^3 + K_{54}S^2 + K_{55}S + K_{56}}$$

where

$K_{43} = 3.35\times10^{-17}$
$K_{44} = 3.78\times10^{-13}$
$K_{45} = 1.06\times10^{-9}$
$K_{46} = 1.38\times10^{-6}$
$K_{47} = 7.94\times10^{-4}$
$K_{48} = 4.66\times10^{-1}$
$K_{49} = 25.4$
$K_{50} = 5.71\times10^{-18}$
$K_{51} = 6.32\times10^{-14}$
$K_{52} = 1.66\times10^{-10}$
$K_{53} = 1.99\times10^{-7}$
$K_{54} = 9.72\times10^{-5}$
$K_{55} = 7.39\times10^{-2}$
$K_{56} = 3.52$

APPENDIX F

M-1 START AND SHUTDOWN SEQUENCES

Start Sequence

At arm switch on, the propellant utilization valve is at 22.2 percent of its steady-state open area. The fuel pump circulation valve (recirculation valve) is open (spring loaded). Automatic sequencing controls control the engine startup as follows:

(1) At fire switch one, the start valve is opened, and the gas generator valve pilot valve, thrust chamber, and gas generator igniters are energized. The propellant utilization valve starts moving toward its steady-state position.

(2) High pressure helium gas is admitted to the turbines initiating pump rotation.

(3) The thrust chamber valve opening is initiated by pump discharge pressures.

(4) The gas generator valves are actuated by increasing hydrogen pressure taken from the gas generator propellant line. A timing orifice controls the opening rate.

(5) Propellants enter the gas generator combustion chamber and are ignited.

(6) Propellants enter the thrust chamber combustion chamber and are ignited.

(7) Rising fuel pump discharge pressure closes the spring loaded fuel pump circulation valve.

(8) As gas generator chamber pressure increases, the helium check valve is closed, which terminates the helium flow from the start bottle to the turbines.

(9) The start valve is closed at 90-percent-rated thrust chamber pressure, which vents the helium start lines.

(10) The gas generator and thrust chamber igniters are deenergized at 90-percent-rated thrust chamber pressure.

(11) The engine bootstraps to its rated operating conditions.

Shutdown Sequence

After an initiating input signal, automatic sequencing controls control the shutdown as follows:

(1) The shutdown signal deenergizes the gas generator valve pilot valve to the vent position, which vents the actuator and allows spring forces to close the valves.

(2) The closing of the gas generator valves stops the flow of propellants to the gas generator and, consequently, the supplying of drive gases to the pump turbines.

(3) With a loss of driving power, the pumps begin decelerating and the discharge pressures decay.

(4) Decaying pump pressures allow spring forces to close the thrust chamber valves and open the recirculation valve.

(5) As the thrust chamber and gas generator valves close and propellant flow is shut-off, the turbopumps stop and engine operation is terminated.

REFERENCES

1. Wanhainen, John P.; Antl, Robert J.; Hannum, Ned P.; and Mansour, Ali H.: Throttling Characteristics of a Hydrogen-Oxygen, Regeneratively Cooled, Pump-Fed Rocket Engine. NASA TM X-1043, 1964.

2. Beckenbach, Edwin F., ed.: Modern Mathematics for the Engineer. McGraw-Hill Book Co., Inc., 1956.

3. Vennard, John K.: Elementary Fluid Mechanics. Third ed., John Wiley and Sons, Inc., 1954.

4. Shapiro, Ascher H.: The Dynamics and Thermodynamics of Compressible Fluid Flow. Vol. I. Ronald Press Co., 1953.

5. McAdams, William H.: Heat Transmission. Third ed., McGraw-Hill Book Co., Inc., 1954.

6. Priem, Richard J.; and Heidmann, Marcus F.: Propellant Vaporization as a Design Criterion for Rocket-Engine Combustion Chambers, NASA TR R-67, 1960.

"The aeronautical and space activities of the United States shall be conducted so as to contribute . . . to the expansion of human knowledge of phenomena in the atmosphere and space. The Administration shall provide for the widest practicable and appropriate dissemination of information concerning its activities and the results thereof."

—NATIONAL AERONAUTICS AND SPACE ACT OF 1958

NASA SCIENTIFIC AND TECHNICAL PUBLICATIONS

TECHNICAL REPORTS: Scientific and technical information considered important, complete, and a lasting contribution to existing knowledge.

TECHNICAL NOTES: Information less broad in scope but nevertheless of importance as a contribution to existing knowledge.

TECHNICAL MEMORANDUMS: Information receiving limited distribution because of preliminary data, security classification, or other reasons.

CONTRACTOR REPORTS: Technical information generated in connection with a NASA contract or grant and released under NASA auspices.

TECHNICAL TRANSLATIONS: Information published in a foreign language considered to merit NASA distribution in English.

TECHNICAL REPRINTS: Information derived from NASA activities and initially published in the form of journal articles.

SPECIAL PUBLICATIONS: Information derived from or of value to NASA activities but not necessarily reporting the results of individual NASA-programmed scientific efforts. Publications include conference proceedings, monographs, data compilations, handbooks, sourcebooks, and special bibliographies.

Details on the availability of these publications may be obtained from:

SCIENTIFIC AND TECHNICAL INFORMATION DIVISION

NATIONAL AERONAUTICS AND SPACE ADMINISTRATION

Washington, D.C. 20546